Electron-Doping-Enhanced High-temperature Superconductivity in (3,0) Carbon Nanotube

Shu-Xiang Qiao (乔树祥),[1] Ya-Ping Li (李牙平),[1] Jin-Han Tan (谭锦函),[1] Na Jiao (焦娜),[1] Meng-Meng Zheng (郑萌萌),[1] Hong-Yan Lu (路洪艳),[1,*] and Ping Zhang (张平)[1,2,†]

[1] *School of Physics and Physical Engineering, Qufu Normal University, Qufu 273165, China*
[2] *Institute of Applied Physics and Computational Mathematics, Beijing 100088, China*

(Dated: September 27, 2026)

Carbon-based materials provide a fertile ground for exploring emergent quantum phenomena. Recently, three-dimensional networks of ultrathin (3,0) and (2,1) carbon nanotubes (CNTs) confined in zeolite pores have been experimentally reported to exhibit room-temperature superconductivity. Given the instability of the (2,1) CNT, we perform first-principles calculations of superconductivity in (3,0) CNT. The predicted superconducting transition temperature (T_c) of the pristine (3,0) CNT is 18.8 K, and Li doping further increases T_c to 25.7 K. Remarkably, electron doping at 0.5 e/cell enhances the density of states and induces significant phonon softening, raising T_c to 45.6 K, exceeding the McMillan limit and surpassing several reported CNT-based superconductors, although it still can not achieve the experimentally reported room-temperature superconductivity. This work advances understanding of superconductivity in one-dimensional carbon materials and suggests a route toward high-T_c superconductivity in carbon nanostructures.

Keywords: Superconductivity; Carbon nanotube; Electron Doped
PACS: 74.20.Fg; 73.63.Fg; 74.72.Ek

I. INTRODUCTION

Superconductors have continuously stimulated the scientific community's sustained interest since the discovery of superconductivity, owing to their zero resistance and complete diamagnetism [1–5]. Given the diversity of structures and electronic properties, exploring superconductivity in carbon-based materials has attracted considerable attention. Studies of superconductivity in three-dimensional (3D) graphite and two-dimensional (2D) graphene, enabled by doping and other approaches, have greatly deepened our understanding of the carbon-based materials. For example, intercalating Ca [6], Ba [7], or Na [8] can render graphite intercalation compounds superconducting. Graphene can exhibit superconductivity under hole doping and biaxial tensile strain [9]. The adsorption of Li [10], Ca [11], or Al [12] adatoms on graphene can also induce superconductivity.

Besides these 2D and 3D carbon systems, the exploration of superconductivity has extended into the realm of one-dimensional (1D) carbon nanostructures. Carbon nanotubes (CNTs) exhibit characteristic physical properties of 1D systems, making them an excellent platform for investigating low-dimensional quantum phenomena. The successful synthesis and functionalization of CNTs have also had a significant impact on nanotechnology and related technological applications [13–16]. Previous experimental studies have demonstrated that CNTs, such as (5,0), (3,3), and (4,2) CNTs, can be synthesized in the channels of zeolite crystals [17, 18]. Additionally, superconductivity in CNTs has been extensively investigated. The experimentally reported superconducting transition temperatures (T_cs) in CNTs are generally below 15 K [19–21]. A previous study showed that the (3,3) CNT is a Dirac semimetal, where a Peierls instability suppresses superconductivity [22]. Subsequent theoretical works reveal that doping (3,3) CNTs with In, Al, Si, or La atoms can turn them into 1D superconductors with T_c ranging from 17 K to 29 K [23]. However, the T_c of these superconducting CNTs remain below the McMillan limit.

The recent experimental work reported possible high-T_c superconductivity in B-doped (hole-doped) ultrathin (3,0) and (2,1) CNTs confined in zeolite pores [24]. In their work, calculations also indicate that the isolated (2,1) CNT exhibits imaginary phonon modes, whereas the (3,0) CNT is dynamically stable [24]. However, the microscopic mechanism and the role of doping remain unclear. In a recent theoretical work, pristine and 1.3 holes/cell doped (3,0) CNTs are predicted to be superconductors with T_c of 18.13 and 5.21 K, respectively [25]. It is found that the hole doping will reduce the superconductivity, which provides a new view. In addition, whether electron doping can enhance T_c is worth exploring. Therefore, we investigate the effect of electron doping (both via Li intercalation and uniform electron addition) on the superconductivity of the (3,0) CNTs. These will provide a complementary theoretical perspective and offer a different route for experimental exploration.

* hylu@qfnu.edu.cn
† zhang_ping@iapcm.ac.cn

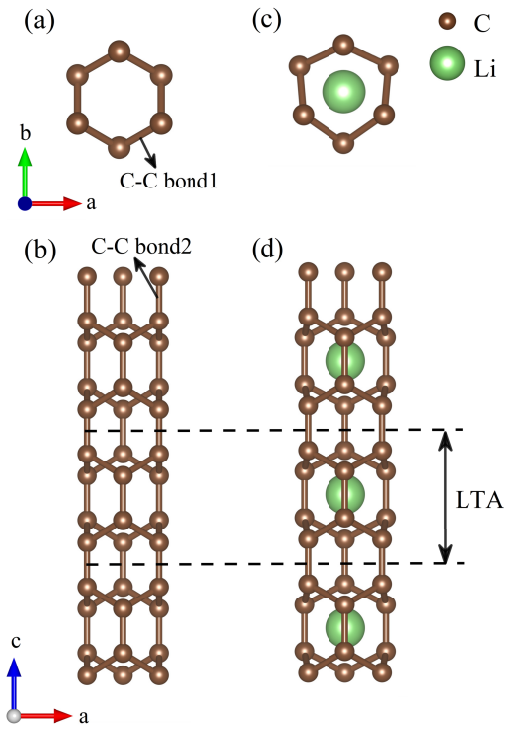


Fig. 1. (a) Top and (b) side views of the pristine (3,0) CNT. (c)-(d) are similar with (a)-(b) but for Li-doped (3,0) CNT. The bond1 is the inclined C-C bond with a finite circumferential component, whereas bond2 is parallel to the nanotube axis.

In this work, we theoretically study the enhanced superconductivity by electron doping in the (3,0) CNT. The results indicate that the pristine (3,0) CNT is metallic and exhibits dynamic stability. We predict an intrinsic T_c of 18.8 K with $\lambda = 0.68$. Under Li doping, the (3,0) CNT remains dynamically stable, with the electron-phonon coupling (EPC) constant λ and T_c calculated to be 1.15 and 25.7 K, respectively. Furthermore, at an electron doping level of 0.5 e per unit cell, the density of states (DOS) at the Fermi level $N(E_F)$ increases and the phonon spectrum exhibits notable softening. Then, the EPC constant λ increases to 1.86, and the T_c increases to 45.6 K. This value exceeds the pristine, and Li-doped (3,0) CNTs. Therefore, the doped (3,0) CNT proposed in this study serves as a promising platform for high T_c 1D superconductivity and offers valuable theoretical guidance for future experimental efforts.

II. METHODS

All calculations in this study were based on the framework of density functional theory (DFT), using the Vienna ab-initio simulation package (VASP) [35] and the QUANTUM-ESPRESSO (QE) software [36]. The generalized gradient approximation (GGA) with the Perdew-Burke-Ernzerhof (PBE) form [37] was used to describe exchange-correlation effects, while electron-ion interactions were described via the projector augmented-wave (PAW) method [38]. VASP was used for structural relaxation, electronic structures, and ab-initio molecular dynamics (AIMD) simulations [35], whereas Quantum ESPRESSO was used for density-functional perturbation theory phonon calculations, the Eliashberg spectral function, superconductivity properties, and the electron–phonon coupling parameters [36]. Other calculation details related parameters are included in the Supplementary Materials (SM).

III. RESULTS AND DISCUSSIONS

A. Crystal structures and stability

Figure 1 illustrates the top and side views of the pristine and Li-doped (3,0) CNTs. As shown in Fig. 1(a), the pristine (3,0) CNT is a zigzag-type structure with a small diameter, making it one of the thinnest stable CNTs. From the side view, presented in Fig. 1(b), it exhibits an almost ideal cylindrical geometry. In the (3,0) CNT, two types of C-C bond lengths are present: C-C bond1 and C-C bond2 with lengths of 1.49 and 1.41 Å. The carbon atoms

form slightly distorted C-C bonds compared with graphene, which is a consequence of the strong curvature inherent to ultrafine CNTs. In addition, we define the nanotube diameter as the maximum distance between the centers of two opposite C atoms after projection onto the plane perpendicular to the tube axis. For the pristine (3,0) CNT, the calculated diameter and the translational vector length along the tube axis direction (LTA) are 2.63 and 4.22 Å, respectively.

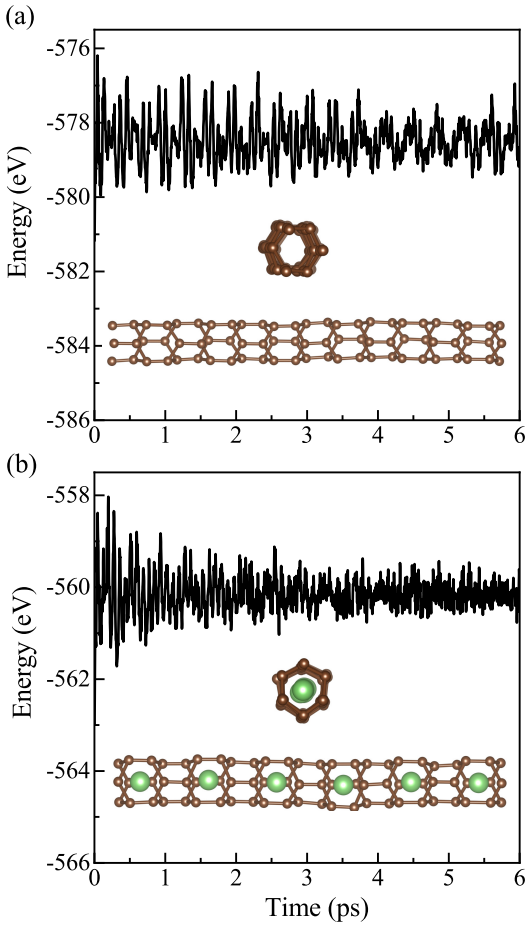


Fig. 2. The variation of the free energy in the AIMD simulations during the time scale of 6 ps along with the last frame of photographs at 300 K for (a) pristine and (b) Li-doped (3,0) CNT.

To determine the preferred Li position, we displaced Li radially by 0.2-0.5 Å from the tube axis and fully relaxed the resulting structures. In every case, Li returned to the axial position. We also compared this configuration with relaxed external top, bridge, and hollow adsorption geometries. The internal on-axis structure was lower in energy, confirming that it is the lowest-energy configuration among the sites examined at the LiC_{12} composition and primitive-cell periodicity. Upon Li doping, Li atoms are accommodated in the hollow core and align along the tube axis, forming a 1D Li intercalant chain that only slightly perturbs the carbon framework, and the optimized nearest-neighbor Li-Li distance is 4.19 Å. As shown in Figs. 1(c) and 1(d), Li doping leads to a slight increase in the tube diameter. Upon Li doped, the tube diameter changes to 2.84 Å. The corresponding bond1 and bond2 lengths are 1.56 and 1.46 Å, respectively.

To quantify the charge transfer between Li and CNT, we performed a Bader charge analysis for the optimized Li-doped structure. Each Li atom donates approximately 0.66 e to the CNT. The six C atoms closest to Li gain approximately 0.09 e/atom, whereas the other six C atoms gain approximately 0.02 e/atom. This Bader-derived value represents a nominal real-space charge transfer and should not be equated directly with the number of electrons introduced in the uniform-doping calculations. For other alkali metals and alkaline earth metals doping, through our calculations, it is found that due to the relatively small diameter of (3,0) CNT, other alkali metals with larger radius cannot exist inside them, which leads to higher lattice strain and ultimately destroys their tubular structure. Therefore, we will not continue to consider the calculation of other alkali metals doping cases.

To further assess the thermal stability and dynamical stability, *ab initio* molecular dynamics (AIMD) simulations and phonon spectra calculations are performed. As shown in Fig. 2, both pristine and Li-doped (3,0) CNTs remain

close to their initial configurations with no significant structural distortion during a 6 ps simulation at 300 K, indicating good thermal stability. Additionally, the phonon spectra of the pristine (Fig. 4(a)) and Li-doped (3,0) (Fig. 4(e)) CNTs show no imaginary frequencies, confirming their dynamical stability. The phonon dispersion and EPC are discussed in detail below. These stability analyses provide theoretical support for the experimental feasibility of synthesizing these CNT structures and exploring their properties.

B. Electronic structures

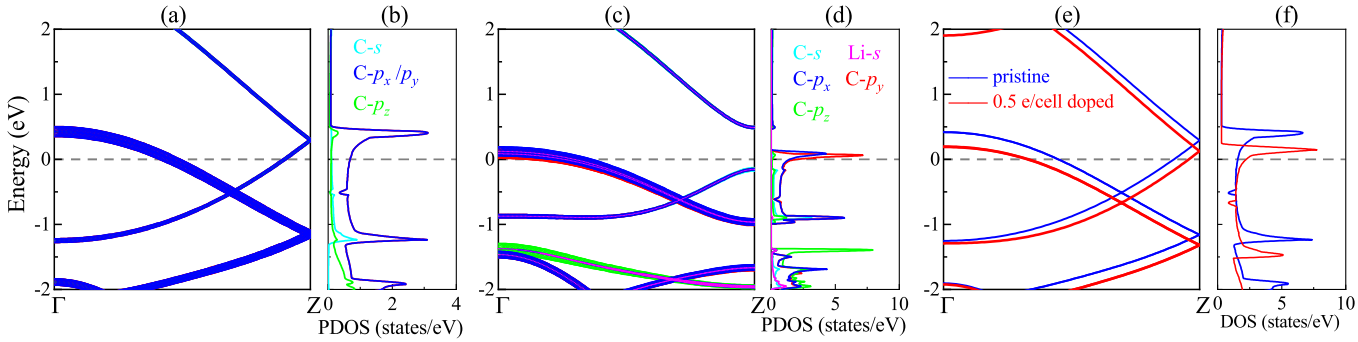


Fig. 3. (a) Orbital-projected band and (b) PDOS of pristine (3,0) CNT. (c)-(d) are similar with (a)-(b) but for Li-doped (3,0) CNT. (e) Band structures and (f) DOS for pristine (blue) and 0.5 e/cell doped (red) (3,0) CNT.

Electronic structure is crucial for understanding the physical properties and the mechanism of superconductivity. Figure 3 shows the band structures and DOS of pristine, Li-doped, and 0.5 e/cell electron-doped (3,0) CNTs. For the pristine (3,0) CNT, Figs. 3(a) and 3(b) show the band structure and projected density of states (PDOS), revealing that it is metallic, with two bands crossing the Fermi level along Γ-Z direction. The PDOS shows strong contributions from C-p_x/p_y orbitals near the Fermi level, suggesting that partially occupied σ-bonding states contribute to the metallic behavior and play an important role in the EPC and superconductivity [26, 27]. We also note that no gap opening associated with a Peierls instability is found in our calculations, in contrast to (3,3) CNTs [22].

Lithium, as a strong electron donor, transfers its valence electrons to the (3,0) CNT, leading to effective n-type doping. Upon Li doping, as shown in Figs. 3(c) and 3(d), the nearly flat bands emerge near the Fermi level, resulting in an enhanced DOS at the Fermi level $N(E_F)$. The electronic states at the Fermi level are dominated by C-p_x and p_y orbitals, while the contribution from Li-s orbitals is negligible. Li incorporation not only provides charge carriers, but also modifies the band dispersion through its interaction with the carbon framework, thereby facilitating enhanced EPC. Moreover, electron doping shifts the Fermi level into a high-DOS region, giving rise to a pronounced peak in the DOS.

At the electron doping level of 0.6 e/cell, the (3,0) CNT becomes dynamically unstable (see Fig. S1 of the SM). The harmonic phonon dispersion develops an imaginary branch centered near Γ, indicating that electron doping has driven the CNT beyond its dynamical-stability boundary. However, the present results do not establish a Peierls or CDW transition, because a $2k_{\mathrm{F}}$ anomaly, a lower-energy symmetry-broken supercell, and an associated periodic charge modulation or electronic gap have not been demonstrated. Therefore, we refer to it as a doping-induced lattice instability. A competing distorted phase at higher doping cannot be excluded.

Thus, we focus on the case of 0.5 e/cell electron doping. Figures 3(e) and 3(f) compare the band structures and DOS of the pristine (blue) and 0.5 e/cell doped (red) cases, highlighting a pronounced evolution of the electronic structure when an additional 0.5 e per unit cell is introduced. At 0.5 e per unit cell, the Fermi level shifts upward and the DOS increases markedly compared to the case of pristine (3,0) CNT. This enhanced DOS is a key prerequisite for strengthening EPC and creates an electronic environment favorable for phonon-mediated pairing within the EPC framework.

C. EPC and superconductivity

The superconducting properties of the pristine, Li-doped, and 0.5 e/cell doped (3,0) CNTs are analyzed using phonon dispersion weighted by the magnitude of $\lambda_{\mathbf{q}\nu}$, phonon dispersion weighted by the vibration modes of each atom, phonon density of states (PhDOS), Eliashberg spectral function $\alpha^2F(\omega)$, and EPC $\lambda(\omega)$, as shown in Fig. 4. No imaginary frequencies are observed in the phonon spectra, indicating that all three structures are dynamically

stable. In the pristine (3,0) CNT, the primitive cell contains 12 atoms, giving rise to 36 phonon branches with a maximum frequency of 1519 cm^{-1}. As shown in Fig. 4(a), the slight splitting of the two lowest acoustic branches near the Γ point originates from tiny numerical symmetry breaking in the fully relaxed structure and finite computational accuracy. In addition, Figure 4(a) also shows that low-frequency phonons (200-400 cm^{-1}) near the Γ and Z points dominate the EPC. These phonon modes are primarily associated with radial C-xy vibrations, thereby contributing more strongly to the EPC than other vibrational modes, as shown in Fig. 4(b). Figure 4(d) further reveals that the coupling between σ electrons and radial vibration phonon modes of the C atoms accounts for approximately 75 % of the total EPC λ. The calculated EPC constant λ and the T_c of pristine (3,0) CNT are 0.68 and 18.8 K, respectively, in good agreement with recent results [25].

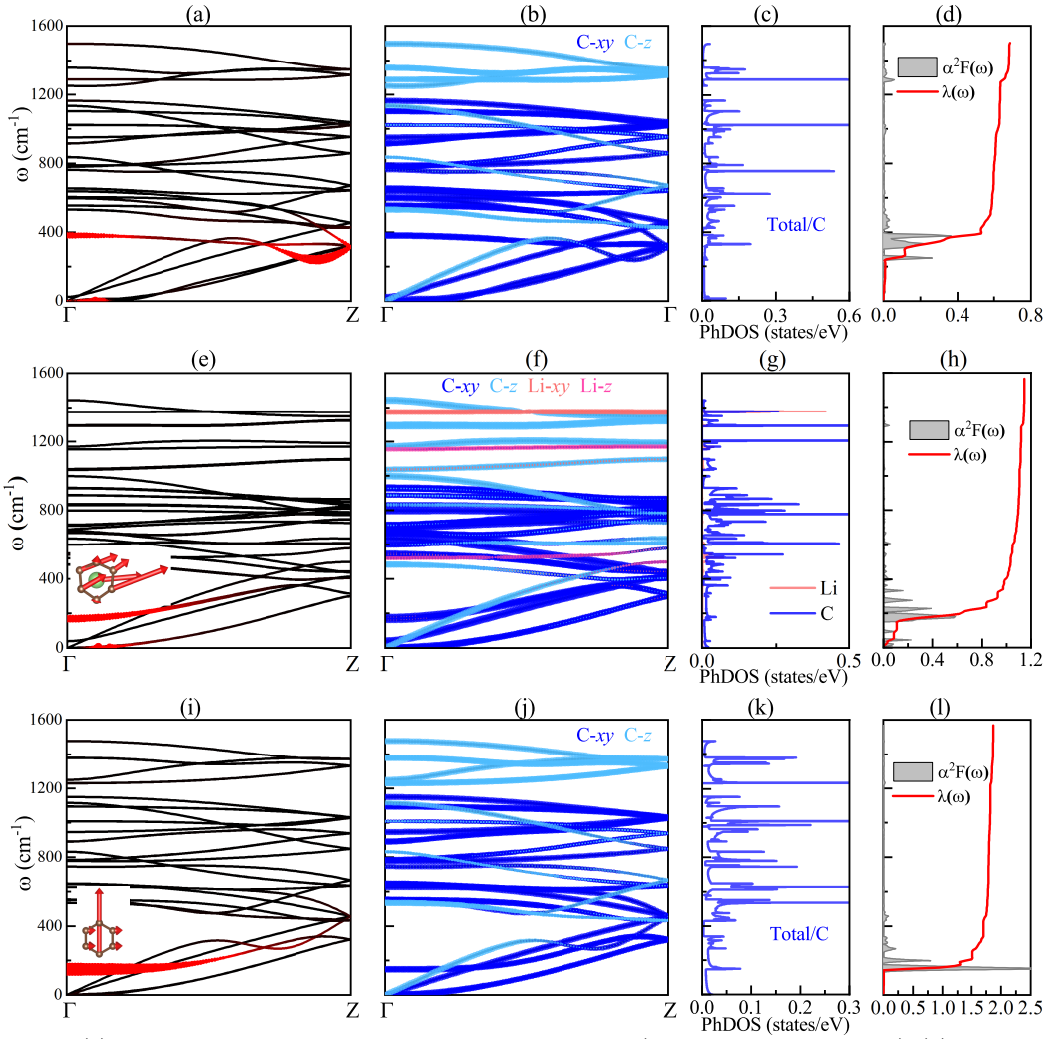


Fig. 4. (a) Phonon dispersion weighted by the magnitude of $\lambda_{\mathbf{q}\nu}$ (EPC for phonon mode $\mathbf{q}\nu$), (b) phonon dispersion weighted by the vibration modes of each atoms, (c) PhDOS, and (d) Eliashberg spectral function $\alpha^2F(\omega)$, and EPC $\lambda(\omega)$ for pristine (3,0) CNT. (e)-(h) and (i)-(l) are similar with (a)-(d) but for Li-doped and 0.5 e/cell electron-doped (3,0) CNT. The insets show the vibration modes.

For the Li-doped (3,0) CNT, each primitive cell contains 13 atoms, yielding 39 phonon branches. The mode- and atom-projected phonon dispersion in Fig. 4(f), together with the element-resolved PhDOS in Fig. 4(g), shows finite Li displacement weight near approximately 500, 1200, and 1400 cm^{-1}. Because the modes near 1200 and 1400 cm^{-1} also contain substantial C contributions and overlap with the upper carbon phonon manifold, we assign them to mixed C-Li vibrations rather than purely Li-localized modes. Comparison of Figs. 4(a) and 4(e) shows that Li incorporation leads to a softening near Γ and a hardening near Z of low-frequency phonon modes. The EPC is dominated by the low-frequency region (around 200 cm^{-1}), as indicated by the $\lambda_{\mathbf{q}\nu}$-weighted segments in Fig. 4(e). As shown in Figs. 4(f) and 4(g), the strongest EPC originates from radial vibrations of C atoms (See the inset in Fig. 4(e)), accounting for approximately 76 % of the total EPC. These phonon modes couple strongly to the C-p_x and p_y electronic states, thereby increasing λ to 1.15 and raising T_c to 25.7 K. This enhancement is consistent with the increased $N(E_F)$ and the softening of low-frequency phonons, both of which favor stronger EPC.

Subsequently, we investigate the superconducting properties of the 0.5 e/cell doped (3,0) CNT, as shown in Figs. 4(i)-4(l). Electron doping not only modifies the electronic structure but also significantly affects the phonon properties. Compared with the phonon dispersion of pristine (3,0) CNT in Fig. 4(a), the high-frequency phonon region remains nearly unchanged upon electron doping, whereas the low-frequency phonon modes are significantly softened near Γ. As shown in Figs. 4(i) and 4(l), these softened branches provide the dominant contribution to the EPC, accounting for about 89%. This indicates that electron doping substantially enhances the EPC strength, thereby improving the superconducting properties of (3,0) CNT. Furthermore, Fig. 4(j) shows that the softened phonon modes arise primarily from radial vibration of C atoms, as shown in the inset of Fig. 4(i).

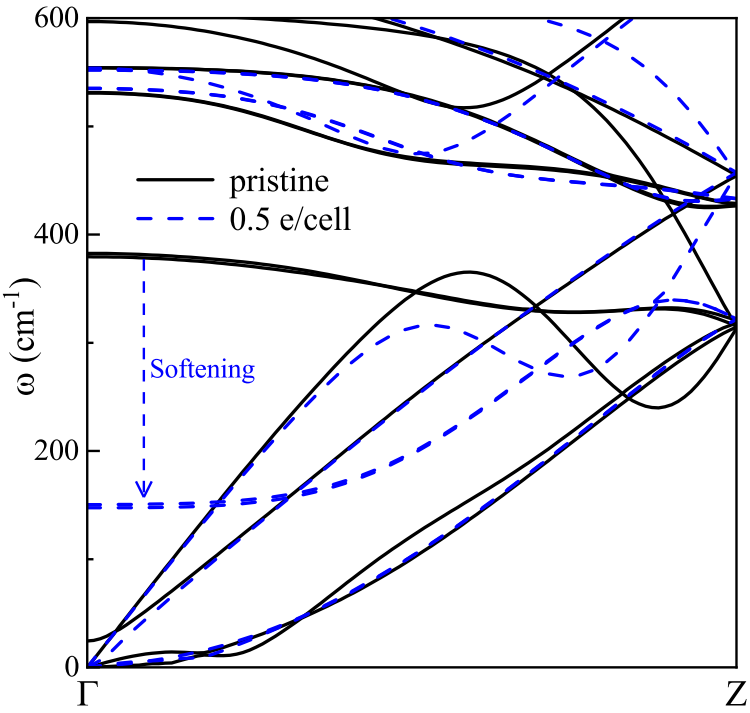


Fig. 5. Phonon dispersions below 600 cm^{-1} of pristine (3,0) CNT (solid black line) and 0.5 e/cell doped (3,0) CNT (dashed blue lines).

As a result of electron doping, the EPC is significantly enhanced, with the total EPC λ increasing from 0.68 to 1.86. This sharp increase is primarily driven by the pronounced softening of low-frequency phonons upon doping, as reported in doped-hydrogenated (5,5) CNT [29]. Upon electron doping, the phonon frequency near Γ decreases markedly from around 380 to around 150 cm^{-1}, as highlighted by the arrow in Fig. 5. Given the large EPC strength ($\lambda = 1.86$), we consider the strong-coupling correction factor f_1 and shape correction factor f_2, which are 1.12 and 1.08, respectively. Using the Allen–Dynes modified McMillan formula [30], the resulting T_c reaches 45.6 K. Although this formulation extends the original McMillan equation into the strong-coupling regime, the resulting T_c remains an approximate harmonic mean-field estimate. In the present case, most of the enhancement of λ arises from a soft phonon branch close to a structural instability. Anharmonic renormalization may harden and stabilize this mode, reducing its contribution to λ, or may favor a symmetry-broken phase that competes with superconductivity. Moreover, because the equilibrium geometry, band positions, density of states, and phonon force constants are evaluated using PBE, the precise critical doping, λ, and T_c may depend on the exchange-correlation functional. Quantitative confirmation will require anharmonic phonons, comparison between exchange-correlation functionals, and a numerical momentum-dependent Eliashberg treatment.

The superconducting parameters obtained in this work for the (3,0) CNTs are summarized in Table 1. Among the uniformly doped systems considered here, T_c reaches its maximum value of 45.6 K at 0.5 e/cell, while the structure becomes dynamically unstable at 0.6 e/cell. Although the Bader-derived charge transfer in the Li-doped system is approximately 0.66 e/cell, the transferred charge is strongly nonuniform and the explicit Li ions modify the local potential, electronic hybridization, equilibrium structure, and interatomic force constants. Consequently, the Li-doped nanotube is not equivalent to a uniformly doped nanotube with 0.66 electrons per cell. These differences account for its dynamical stability and its comparatively smaller λ and T_c. To ensure the reliability of these conclusions, we carried out systematic k and q-mesh convergence tests for EPC calculations to confirm that the λ values are not an artifact of coarse sampling, as shown in Fig. S2 of the SM. At the adopted Gaussian broadening of 0.02 Ry, the calculated λ values obtained using these meshes differ by no more than approximately 2%. When the Gaussian broadening is

varied from 0.01 to 0.03 Ry, λ changes by approximately 3% for the pristine CNT, 3-4% for the Li-doped CNT, and 2-3% for the 0.5 e/cell electron-doped CNT.

Table 1. Atomic or charge doping, $N(E_F)$ (states/(spin Ry/cell)), logarithmically averaged phonon frequency ω_{log} (K), EPC constant λ, and superconducting T_c (K) for pristine, Li-doped, and 0.5 e/cell electron-doped (3,0) CNT superconductors in this work.

CNTs	doping	$N(E_F)$	ω_{log}	λ	T_c
(3,0) CNT	0	21.36	567	0.68	18.8
(3,0) CNT	Li	22.42	300	1.15	25.7
(3,0) CNT	0.5 e/cell	25.71	278	1.86	45.6

The present calculation is that it describes an isolated, periodic (3,0) CNT at ambient pressure. Therefore, the calculated Tc represents the mean-field pair-formation scale obtained within the isotropic electron-phonon framework. In the thermodynamic limit, a strictly one-dimensional system with short-range interactions cannot sustain true finite-temperature long-range order associated with a continuous symmetry. In a finite quasi-one-dimensional superconducting wire, thermally activated and quantum phase slips may further reduce the phase-ordering temperature and generate a finite resistance. A Berezinskii-Kosterlitz-Thouless-type transition would require an effectively two-dimensional coupled geometry, whereas intertube or Josephson coupling in a three-dimensional CNT network can provide transverse phase stiffness and stabilize bulk phase coherence through a dimensional crossover.

Moreover, B doped can induce local bond relaxation, modified force constants and vibrational modes, impurity-derived electronic states, nonuniform charge transfer, and disorder. The zeolite environment, tube-tube junctions, and applied pressure may also modify the van Hove singularities, phonon spectrum, electron-phonon matrix elements, and intertube coupling. These effects are absent from both the isolated-tube model adopted here and the uniform-hole-doping model of Ref. [25]. Therefore, the reduction of λ does not directly contradict the high-temperature collective behavior reported for the B-doped, zeolite-confined CNT network in Ref. [24]. A quantitative explanation of the much higher temperature scale and its strong pressure dependence in Ref. [24] requires explicit treatment of B substitution, zeolite confinement, pressure, and the full interconnected CNT network.

Importantly, the T_c obtained at 0.5 e/cell doping not only exceeds the McMillan limit (37 K), but also substantially surpasses most previously reported experimental and theoretical T_c values for CNTs, as well as those for several quasi-1D superconductors. For instance, experimental reports of CNT superconductivity include rope-like single-walled CNTs (0.55 K) [20], multi-walled CNTs (12 K) [21], and single-walled CNTs in zeolites (15 K) [19]. The theoretically predicted T_c values of atom-doped (3,3) CNTs and hole-doped (3,0) CNTs are 17-28 K [23] and 5.21 K [25], respectively. Additionally, several quasi-1D superconductors have been reported, including Al (< 1.6 K) [31], Ta_2PdS_5 (3.3 K) [32], Sn (4 K) [33], and NaBe (21.2 K) [34], etc.

Furthermore, the pristine and doped (3,0) CNT can serve as a superconducting unit, where phonon modes with strong EPC can be embedded within larger frameworks or 3D networks, potentially providing a route toward superconductivity in the room-temperature regime under relatively low pressure. Thus, our findings indicate that the (3,0) CNT provides a minimal yet versatile model system for investigating low-dimensionality effects, electronic correlations, and the design of high-T_c 1D superconductors. The present results identify electron-doped (3,0) CNTs as a useful microscopic platform for studying strong electron-phonon pairing in the quasi-one-dimensional limit.

IV. CONCLUSION

In this work, we have conducted a first-principles investigation of the superconducting properties of the (3,0) CNT. Our results predict that the pristine (3,0) CNT exhibits a superconducting T_c of 18.8 K ($\lambda = 0.68$). Its superconducting properties can be further enhanced through Li or electron doping. Li doping noticeably enhances the EPC, yielding λ and T_c are 1.15 and 25.7 K, respectively. Notably, an even stronger enhancement is achieved through electron doping. Electron doping at 0.5 e/cell significantly strengthens the EPC, giving λ of 1.86 and a high T_c of 45.6 K. This T_c value surpasses the McMillan limit and is higher than most previously reported T_c values for CNTs. This substantially elevated transition temperature underscores the capability of this ultrafine nanotube to host strongly enhanced phonon-mediated pairing interactions. Thus, the (3,0) CNT provides a model system for probing fundamental coupling mechanisms in reduced dimensions and offers theoretical guidance for future experimental efforts to manipulate nanotube superconductivity.

ACKNOWLEDGMENTS

This work is supported by the National Natural Science Foundation of China (Grant Nos. 12674304 and 12074213), National Key R&D Program of China (Grant No. 2022YFA1403103), and the Natural Science Foundation of Shandong Province (Grant Nos. ZR2026MS0019 and ZR2023MA082).

[1] Bardeen J, Cooper L N and Schrieffer J R 1957 *Phys. Rev.* **108**(5) 1175–1204 URL https://link.aps.org/doi/10.1103/PhysRev.108.1175

[2] Gor'kov L P and Kresin V Z 2018 *Rev. Mod. Phys.* **90**(1) 011001 URL https://link.aps.org/doi/10.1103/RevModPhys.90.011001

[3] Choi H J, Roundy D, Sun H, Cohen M L and Louie S G 2002 *Nature* **418** 758–760 ISSN 1476-4687 URL https://doi.org/10.1038/nature00898

[4] Aperis A, Maldonado P and Oppeneer P M 2015 *Phys. Rev. B* **92**(5) 054516 URL https://link.aps.org/doi/10.1103/PhysRevB.92.054516

[5] Yildirim T, Gülseren O, Lynn J W, Brown C M, Udovic T J, Huang Q, Rogado N, Regan K A, Hayward M A, Slusky J S, He T, Haas M K, Khalifah P, Inumaru K and Cava R J 2001 *Phys. Rev. Lett.* **87**(3) 037001 URL https://link.aps.org/doi/10.1103/PhysRevLett.87.037001

[6] Emery N, Hérold C, d'Astuto M, Garcia V, Bellin C, Marêché J F, Lagrange P and Loupias G 2005 *Phys. Rev. Lett.* **95**(8) 087003 URL https://link.aps.org/doi/10.1103/PhysRevLett.95.087003

[7] Heguri S, Kawade N, Fujisawa T, Yamaguchi A, Sumiyama A, Tanigaki K and Kobayashi M 2015 *Phys. Rev. Lett.* **114**(24) 247201 URL https://link.aps.org/doi/10.1103/PhysRevLett.114.247201

[8] Ma G, Wang Y, Wang Z, Nakamoto Y, Shimizu K, Liu G, Zhou M, Wang H, Gao P and Ma Y 2025 *Phys. Rev. Lett.* **135**(16) 166003 URL https://link.aps.org/doi/10.1103/2t6l-sqmj

[9] Si C, Liu Z, Duan W and Liu F 2013 *Phys. Rev. Lett.* **111**(19) 196802 URL https://link.aps.org/doi/10.1103/PhysRevLett.111.196802

[10] Ludbrook B M, Levy G, Nigge P, Zonno M, Schneider M, Dvorak D J, Veenstra C N, Zhdanovich S, Wong D, Dosanjh P, Straßer C, Stöhr A, Forti S, Ast C R, Starke U and Damascelli A 2015 *Proc. Natl. Acad. Sci. U. S. A.* **112** 11795–11799 URL https://doi.org/10.1073/pnas.1510435112

[11] Profeta G, Calandra M and Mauri F 2012 *Nat. Phys.* **8** 131–134 ISSN 1745-2481 URL https://doi.org/10.1038/nphys2181

[12] Lu H Y, Yang Y, Hao L, Wang W S, Geng L, Zheng M, Li Y, Jiao N, Zhang P and Ting C S 2020 *Phys. Rev. B* **101**(21) 214514 URL https://link.aps.org/doi/10.1103/PhysRevB.101.214514

[13] Iijima S 1991 *Nature* **354** 56–58 ISSN 1476-4687 URL https://doi.org/10.1038/354056a0

[14] Ebbesen T W and Ajayan P M 1992 *Nature* **358** 220–222 ISSN 1476-4687 URL https://doi.org/10.1038/358220a0

[15] Souza Filho A G, Jorio A, Samsonidze G G, Dresselhaus G, Pimenta M A, Dresselhaus M S, Swan A K, Ünlü M S, Goldberg B B and Saito R 2003 *Phys. Rev. B* **67**(3) 035427 URL https://link.aps.org/doi/10.1103/PhysRevB.67.035427

[16] Sun L, Wang X, Wang Y and Zhang Q 2017 *Carbon* **122** 462–474 ISSN 0008-6223 URL https://www.sciencedirect.com/science/article/pii/S000862231730684X

[17] Wang N, Tang Z K, Li G D and Chen J S 2000 *Nature* **408** 50–51 ISSN 1476-4687 URL https://doi.org/10.1038/35040702

[18] Qin L C, Zhao X, Hirahara K, Miyamoto Y, Ando Y and Iijima S 2000 *Nature* **408** 50–50 ISSN 1476-4687 URL https://doi.org/10.1038/35040699

[19] Tang Z K, Zhang L, Wang N, Zhang X X, Wen G H, Li G D, Wang J N, Chan C T and Sheng P 2001 *Science* **292** 2462–2465 URL https://doi.org/10.1126/science.1060470

[20] Kociak M, Kasumov A Y, Guéron S, Reulet B, Khodos I I, Gorbatov Y B, Volkov V T, Vaccarini L and Bouchiat H 2001 *Phys. Rev. Lett.* **86**(11) 2416–2419 URL https://link.aps.org/doi/10.1103/PhysRevLett.86.2416

[21] Takesue I, Haruyama J, Kobayashi N, Chiashi S, Maruyama S, Sugai T and Shinohara H 2006 *Phys. Rev. Lett.* **96**(5) 057001 URL https://link.aps.org/doi/10.1103/PhysRevLett.96.057001

[22] Connétable D, Rignanese G M, Charlier J C and Blase X 2005 *Phys. Rev. Lett.* **94**(1) 015503 URL https://link.aps.org/doi/10.1103/PhysRevLett.94.015503

[23] Bo T, Wang Y, Liang Y, Liu X, Ren J, Weng H, Liu M and Meng S 2021 *J. Phys. Chem. Lett.* **12** 6667–6675 URL https://doi.org/10.1021/acs.jpclett.1c02000

[24] Wang Y, Koo T H, Huang R, Ng Y H, Lortz T T, Zhang T, Chan W M, Hou Y, Pan J, Lortz R, Wang N and Sheng P 2025 (*Preprint* 2509.19255) URL https://arxiv.org/abs/2509.19255

[25] Ouyang Z, Jiang J, Zhang J F, Gao M, Liu K and Lu Z Y 2025 (*Preprint* 2511.03764) URL https://arxiv.org/abs/2511.03764

[26] Gao M, Lu Z Y and Xiang T 2015 *Physics* **44** 421–426 ISSN 0379-4148 URL https://wuli.iphy.ac.cn/cn/article/doi/10.7693/wl20150701

[27] Gao M, Lu Z Y and Xiang T 2015 *Phys. Rev. B* **91**(4) 045132 URL https://link.aps.org/doi/10.1103/PhysRevB.91.045132

[28] See Supplemental Material for calculation details, phonon spectra of 0.6 e-doped (3,0) CNT, λ and t_c as a function of degauss for different k meshes and q meshes for pristine, li-doped and 0.5 e/cell electron-doped (3,0) cnts. The Supplemental Material also contains Refs. [35–41].

[29] Wang H, Liu B T, Qiao S X, Jiao N, Yu G, Zhang P, Ting C S and Lu H Y 2026 *Chin. Phys. Lett.* **43** 010706–010706 URL http://cpl.iphy.ac.cn/en/article/doi/10.1088/0256-307X/43/1/010706

[30] Allen P B and Dynes R C 1975 *Phys. Rev. B* **12**(3) 905–922 URL https://link.aps.org/doi/10.1103/PhysRevB.12.905

[31] Altomare F, Chang A M, Melloch M R, Hong Y and Tu C W 2006 *Phys. Rev. Lett.* **97**(1) 017001 URL https://link.aps.org/doi/10.1103/PhysRevLett.97.017001

[32] Zhang E, Zhi J, Zou Y C, Ye Z, Ai L, Shi J, Huang C, Liu S, Lin Z, Zheng X, Kang N, Xu H, Wang W, He L, Zou J, Liu J, Mao Z and Xiu F 2018 *Nature Communications* **9** 4656 ISSN 2041-1723 URL https://doi.org/10.1038/s41467-018-07123-y

[33] Lozano D P, Couet S, Petermann C, Hamoir G, Jochum J K, Picot T, Menéndez E, Houben K, Joly V, Antohe V A, Hu M Y, Leu B M, Alatas A, Said A H, Roelants S, Partoens B, Milošević M V, Peeters F M, Piraux L, Van de Vondel J, Vantomme A, Temst K and Van Bael M J 2019 *Phys. Rev. B* **99**(6) 064512 URL https://link.aps.org/doi/10.1103/PhysRevB.99.064512

[34] Dong W H, Si C, Duan W and Xu Y 2024 *Phys. Rev. Lett.* **133**(23) 236001 URL https://link.aps.org/doi/10.1103/PhysRevLett.133.236001

[35] Kresse G and Furthmüller J 1996 *Phys. Rev. B* **54**(16) 11169–11186 URL https://link.aps.org/doi/10.1103/PhysRevB.54.11169

[36] Giannozzi P, Baroni S, Bonini N, Calandra M, Car R, Cavazzoni C, Ceresoli D, Chiarotti G L, Cococcioni M, Dabo I, Dal Corso A, de Gironcoli S, Fabris S, Fratesi G, Gebauer R, Gerstmann U, Gougoussis C, Kokalj A, Lazzeri M, Martin-Samos L, Marzari N, Mauri F, Mazzarello R, Paolini S, Pasquarello A, Paulatto L, Sbraccia C, Scandolo S, Sclauzero G, Seitsonen A P, Smogunov A, Umari P and Wentzcovitch R M 2009 *J. Phys.: Condens. Matter* **21** 395502 ISSN 0953-8984 URL https://dx.doi.org/10.1088/0953-8984/21/39/395502

[37] Perdew J P, Burke K and Ernzerhof M 1996 *Phys. Rev. Lett.* **77**(18) 3865–3868 URL https://link.aps.org/doi/10.1103/PhysRevLett.77.3865

[38] Kresse G and Joubert D 1999 *Phys. Rev. B* **59**(3) 1758–1775 URL https://link.aps.org/doi/10.1103/PhysRevB.59.1758

[39] McMillan W L 1968 *Phys. Rev.* **167**(2) 331–344 URL https://link.aps.org/doi/10.1103/PhysRev.167.331

[40] Dynes R C 1972 *Solid State Commun.* **10** 615–618 ISSN 0038-1098 URL https://www.sciencedirect.com/science/article/pii/0038109872906035

[41] Kortus J, Mazin I I, Belashchenko K D, Antropov V P and Boyer L L 2001 *Phys. Rev. Lett.* **86**(20) 4656–4659 URL https://link.aps.org/doi/10.1103/PhysRevLett.86.4656